Spin Pumping in Asymmetric $Fe_{50}Pt_{50}$/Cu/$Fe_{20}Ni_{80}$ Trilayer Structure

R. Medwal[1,2*], S. Gupta[2**], R. S. Rawat[1], S. Annapoorni[3], and Y. Fukuma[2]

[1]*Natural Science and Science Education, National Institute of Education, Nanyang Technological University, 637616, Singapore*
[2]*Graduate School of Computer Science and System Engineering, Kyushu Institute of Technology, 680-4 Kawazu, Iizuka 820-8502, Japan*
[3]*Department of Physics and Astrophysics, University of Delhi, 110007, India*

Abstract—We report spin transport dynamics across asymmetric $Fe_{50}Pt_{50}$/Cu/$Fe_{20}Ni_{80}$ soft-magnetic tri-layer structure and thereby determine modulation of magnetic parameters including damping and effective field by means of the angular dependence of broadband ferromagnetic resonance measurements. At distinct precession of individual magnetic layer, spin-pumping is found to be prevalent with expected linewidth increase. Mutual precession for wide-range of resonance configuration revealed a collective reduction in anisotropy field of around 200 mT for both $Fe_{50}Pt_{50}$ and $Fe_{20}Ni_{80}$ system. Subsequent observation of no excess interface damping shows the possible control of spin-pumping effect by tuning the net flow of spin current in a multilayer structure. These experimental findings have significance for microwave devices that require tunable anisotropy field in magnetic multilayers.

Index Terms—Ferromagnetic resonance, Spin-pumping, Effective magnetic field,

Correspondence:
*Rohit Medwal
Email: rohit.medwal@nie.edu.sg
**Surbhi Gupta
E-Mail: gupta@cse.kyutech.ac.jp

I. INTRODUCTION

Spin current, the flow of angular momentum carried by electron spins has played a key role in unveiling the spin-dependent phenomena like giant magnetoresistance and spin-torque induced magnetization switching [1-2]. In particular, efficient generation of pure spin current (I_S), and fundamental understanding of allied transport physics in different nano-structures have attracted more technological interest since nano-magnet switching is demonstrated in spin-orbit-torque devices [3,4]. Out of several routes to the pure spin current generation, spin pumping circumvents the constraint of conduction electrons and thus is studied in different electric states of magnetic as well as adjacent layer materials [5-7]. Whereas charge current is required to apply direct to the sample in other mechanisms of non-local spin-injection [8] and spin Hall effect [9], spin-pumping results from non-equilibrium magnetization dynamics that pump angular momentum (spin current) into the adjacent layer. Here, we are motivated to study this spin-current exchange between two ferromagnets in the tri-layer structure of ferromagnetic/normal/ferromagnetic (FM1/NM/FM2) metal system, which is an indispensable element of read-heads [10] and spin transfer torque nano-oscillators [11]. Interestingly, several experimental outcomes of spin pumping investigation in FM1/NM/FM2 systems are reported: dynamic long-range spin-exchange coupling [12], mutual orientation (parallel and antiparallel) and bias field dependent damping [13], additional anticipated effect of domain wall coupling [14], spin relaxation anisotropy in longitudinal versus transverse geometry [15], anisotropic absorption of pure spin current [16] and many more [17]. But collective dynamics of these magnetic multilayers are essentially probed to grasp new insights of spin relaxation mechanism only, while the concomitant exploration of an interplay between collective dynamics and effective magnetic field in such multilayers remains elusive.

Spin pumping describes, how precessing magnetization vector in FM emits spin momentum to adjacent NM layer, called spin sink, at the price of increased damping (spin relaxation) as defined by the third term in Landau-Lifshitz-Gilbert (LLG) equation of motion; $\frac{d\mathbf{m}}{dt} = -\gamma\, m \times H_{eff} + \alpha^0 m \times \frac{d\mathbf{m}}{dt} + \alpha' \, m \times \frac{d\mathbf{m}}{dt}$ [18]. Where **m** defines the time-varying magnetization, γ is the gyromagnetic ratio of electrons and H_{eff} is an effective magnetic field, including the external, demagnetization and crystal anisotropy field. The intrinsic Gilbert damping α^0 is the timescale at which magnetization **m** aligns to H_{eff} with the additional factor of α' due to the loss of coherently precessing spins, determined by the spin-flip probability of adjacent NM layer, Also, momentum transfer efficiency from precessing magnetization to NM layer parameterized by spin mixing conductance, $g^{\uparrow\downarrow}$, of the FM/NM interface, which can be directly estimated from an increase in α^0, saturation magnetization and spin diffusion length of NM. In a similar fashion, non-local perturbation effect of spin relaxation in FM1/NM/FM2 system with collinear magnetization is also observed when absorption of the transverse component of spin-current leads to spin-transfer-torque on sink layer magnetization and thereby increases the damping of precession in source layer as shown in Figure 1a.

The LLG equation for this dynamic behavior of ith magnetic layer in the magnetic FM1/NM/FM2 system (here, $Fe_{50}Pt_{50}$/Cu/$Fe_{20}Ni_{80}$) may be defined as $\frac{d\mathbf{m_i}}{dt} = -\gamma\, \mathbf{m_i} \times H_{eff} + \alpha_i^0 \mathbf{m_i} \times \frac{d\mathbf{m_i}}{dt} + \alpha'_{i\to j} \mathbf{m_i} \times \frac{d\mathbf{m_i}}{dt} - \alpha'_{j\to i} \mathbf{m_j} \times \frac{d\mathbf{m_j}}{dt})$, where i(j) stands for $Fe_{50}Pt_{50}$ ($Fe_{20}Ni_{80}$) in the following analysis. Here we have neglected the torque term arising from dipolar or indirect exchange interaction owing to Cu (NM) insertion layer. Ignoring the spin-flip scattering probability at both FM1 (FM2)/NM interfaces and assuming NM to be completely spin transparent, the spin current generated by either of precessing magnetization of FM1(FM2) then, may be written as $I_{S,i}^{Pump} = \frac{h}{8\pi}(g_{i\to j}^{\uparrow\downarrow}\mathbf{m_i} \times \frac{d\mathbf{m_i}}{dt} - g_{j\to i}^{\uparrow\downarrow}\mathbf{m_j} \times \frac{d\mathbf{m_j}}{dt})$, thus providing an additional means of controlling the dynamics of magnetic multilayers. In general, spin pumping is considered as a reciprocal process for symmetric systems with both FM of the same material with a single value of $g^{\uparrow\downarrow}$ common for both interfaces [18]. However, for asymmetric system alike present case, where FM1 and FM2 are designed with different intrinsic parameters (uniaxial and cubic anisotropy, shape anisotropy, saturation magnetization Ms), spin pumping is to be analyzed as a non-reciprocal process with dissimilar values of $g_{FM1\to FM2}^{\uparrow\downarrow}$ and $g_{FM2\to FM1}^{\uparrow\downarrow}$ for the different material interface on each side of the insertion layer [19, 20]. However, a simplified approximation that $g_{FM1\to FM2}^{\uparrow\downarrow} = g_{FM2\to FM1}^{\uparrow\downarrow} = g^{\uparrow\downarrow}$ is also debated in the literature [18, 21]. In this comprehensive study, we performed field-sweep broadband ferromagnetic resonance (FMR) measurements to analyze spin-pumping in soft magnetic and asymmetric $Fe_{50}Pt_{50}$/Cu/$Fe_{20}Ni_{80}$ tri-layer structure. We investigated the angular variation in rf-field excited magnetization dynamics of $Fe_{50}Pt_{50}$ and $Fe_{20}Ni_{80}$ along with their mutual effect on linewidth and resonance field of FMR spectra. The analysis indicates that simultaneous precession conditions not only led to anticipated damping reduction but also resulted in the large tuning of the anisotropy field, which could be useful for multilayer spintronic devices.

II. METHODS AND CHARACTERIZATIONS

Tri-layer sample of $Fe_{50}Pt_{50}$ (40 nm)/Cu (5nm)/$Fe_{20}Ni_{80}$ (20 nm) is prepared by physical vapor deposition technique on naturally oxidized Si substrates at room temperature using high purity $Fe_{50}Pt_{50}$ (99.99 %) and $Fe_{20}Ni_{80}$ (99.99 %) material targets. The $Fe_{50}Pt_{50}$ film in disordered (A1) fcc phase is deposited by sputtering [22]. Thereafter, Cu and $Fe_{20}Ni_{80}$ layers are evaporated sequentially on Si/$Fe_{50}Pt_{50}$ at a fixed rate of 0.05 Å/sec in the e-beam chamber. We purposefully used oblique angle deposition technique to grow $Fe_{20}Ni_{80}$ layer that induced uniaxial magnetic anisotropy of 24 mT [see supplementary figure S1] [23, 24]. Here 5 nm Cu insertion layer is inserted between the $Fe_{50}Pt_{50}$ and $Fe_{20}Ni_{80}$. The Cu layer is chosen due to its large spin diffusion length and negligible spin-dependent scattering [25]. The 5 nm Cu layer also suppress indirect exchange coupling via RKKY interaction as well as direct exchange coupling between ferromagnets [26,27]. In addition, Si/$Fe_{50}Pt_{50}$ (40 nm) and Si/$Fe_{20}Ni_{80}$ (20 nm) are also deposited to distinguish the intrinsic damping of both individual ferromagnets as well as the interface induced anisotropy in $Fe_{50}Pt_{50}$/Cu/$Fe_{20}Ni_{80}$ tri-layer structure.

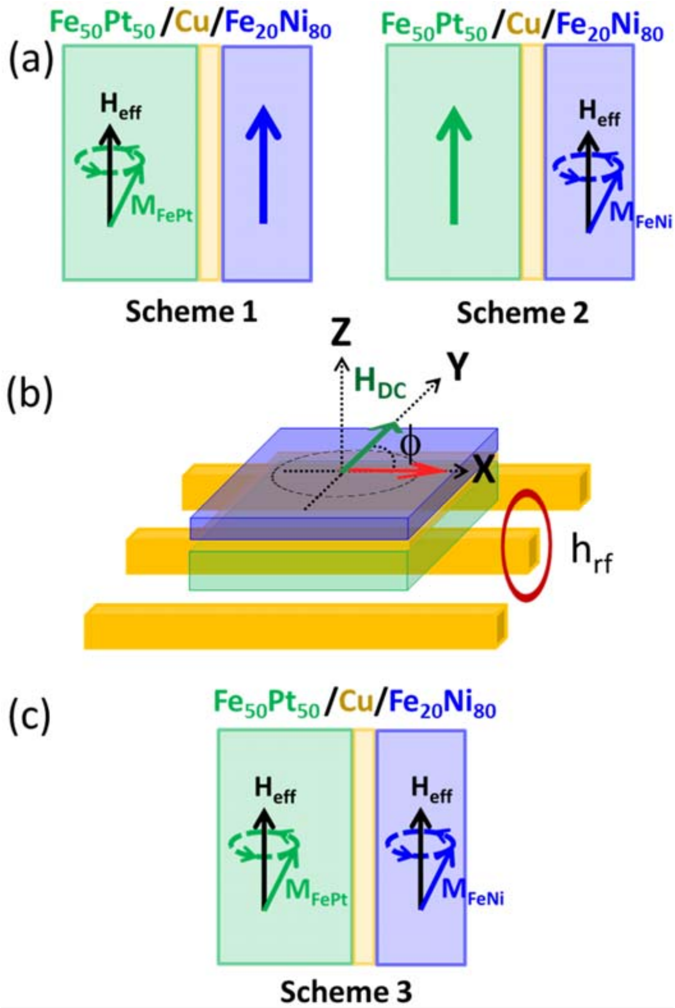

Figure 1. Schematic diagram of a) $Fe_{50}Pt_{50}$/Cu/$Fe_{20}Ni_{80}$ trilayer showing individual magnetization precession in $Fe_{50}Pt_{50}$ (scheme 1) and $Fe_{20}Ni_{80}$ (scheme 2) respectively, b) Flip-chip configuration

for VNA-FMR measurement. Here ϕ is varied between 0 to 120º to analyze c) simultaneous precession (Scheme 3).

All FMR measurements are carried out at room temperature by placing the samples face-down on short-end coplanar waveguide (CPW), designed to have a 50 Ω impedance within a broad frequency range (≤ 20 GHz), as shown in Figure 1b. Vector network analyzer (VNA, Model: Agilent N5222A) is employed to provide rf-field (h_{rf}) which excites the magnetization precession and record the FMR spectra by measuring the complex reflection parameter S_{11}. The external magnetic field H_{DC} is swept in-plane for the fixed frequency range of f = 6-12 GHz while angular dependent FMR measurements are carried out by moving the electromagnets to vary azimuthal angle (ϕ: angle between the static external field and the long axis of CPW). Here purposefully induced in-plane uniaxial anisotropy of $Fe_{20}Ni_{80}$ allows us to measure FMR spectra in a wide range of magnetic field for the collective and individual magnetization precessions in the samples, as can be seen in Figure 1.

III. **RESULTS AND DISCUSSIONS**

Figure 2a and 2b shows real [Re (S_{11})] and imaginary [Im (S_{11})] signal of a typical VNA-FMR spectrum recorded for $Fe_{50}Pt_{50}$/Cu/$Fe_{20}Ni_{80}$ sample at f =7 GHz. Two well-separated resonant peaks centered at ~ 50 mT and ~ 80 mT suggest that when the magnetization of one layer (say $Fe_{50}Pt_{50}$) is precessing at maximum amplitude, the other layer ($Fe_{20}Ni_{80}$) is nearly stationary as shown in scheme 1 and vice versa in scheme 2. Here for each layer, resonance field (H_R) and resonance linewidth (ΔH) is extracted by de-convolution of FMR spectrum into two complex spectra, by fitting with the derivative of the sum of symmetric and antisymmetric Lorentzians, written as [28]

$$F_{S11}(H) = \sum_n \left(L \frac{(\Delta H)^2}{(\Delta H)^2+(H-H_R)^2} + D \frac{\Delta H(H-H_R)}{(\Delta H)^2+(H-H_R)^2} \right) \quad (1)$$

where L and D are the intensity of symmetric and antisymmetric component. Taking summation over L and D for n = 2, accounts for the number of magnetic elements that undergo to FMR. Following the practice for other frequencies, the extracted ΔH values are plotted as a function of f for $Fe_{50}Pt_{50}$ and $Fe_{20}Ni_{80}$ in Fig 2c and 2d respectively. From the slope of anticipated linear dependence, we calculated the effective damping parameter $\alpha^{eff} = \alpha^0 + \alpha'$ using $\mu_o \Delta H = \mu_o \Delta H_o + \frac{2\pi}{\gamma} \alpha^{eff} f$ [21, 29, 30] where the reference value of $\gamma^{Fe_{50}Pt_{50}}$ = 29.5 GHz/T and $\gamma^{Fe_{20}Ni_{80}}$ = 29.5 GHz/T is considered from literature [30, 31]. Noticeable enhancement in damping parameter α^{eff} = 0.015 ± 0.001 and 0.031 ± 0.001 is obtained for $Fe_{20}Ni_{80}$ and $Fe_{50}Pt_{50}$, respectively in multilayer sample ascribed to spin-pumping effect. While uncapped samples Si/$Fe_{20}Ni_{80}$ and Si/$Fe_{50}Pt_{50}$ exhibited smaller values of α° , to be 0.0059 ± 0.0003 and 0.0228 ± 0.0006 respectively [30, 31]. Important to mention that inhomogeneous linewidth (ΔH_o) is found to be slightly increased for $Fe_{20}Ni_{80}$ layer in the tri-layer sample, owing to interface Cu layer roughness with respect to the Si/$Fe_{20}Ni_{80}$ sample. While high ΔH_ovalues are observed for 40 nm thick $Fe_{50}Pt_{50}$ is found to be in accordance with the literature report [31]. The emitted spin current during FMR can be quantified by spin mixing conductance of the Cu/$Fe_{20}Ni_{80}$ and $Fe_{50}Pt_{50}$/Cu interface for the scheme 1 and 2. $\alpha'_{Fe_{50}Pt_{50}} = \alpha'_{Fe_{20}Ni_{80}}$ = 0.009, the spin mixing conductance of Cu/$Fe_{20}Ni_{80}$ and $Fe_{50}Pt_{50}$/Cu interface is estimated to be $g^{\uparrow\downarrow}_{Fe_{50}Pt_{50} \rightarrow Fe_{20}Ni_{80}}$= 2.9 × 10^{19} m^{-2} for the scheme 1 and $g^{\uparrow\downarrow}_{Fe_{20}Ni_{80} \rightarrow Fe_{50}Pt_{50}}$ = 4.0 × 10^{19} m^{-2} for the scheme 2, respectively, for given $\lambda_{Fe_{50}Pt_{50}}$ = 5 nm and $\lambda_{Fe_{20}Ni_{80}}$= 5 nm [32]. $\lambda_{Fe_{50}Pt_{50}}$ and $\lambda_{Fe_{20}Ni_{80}}$ are spin diffusion length of the $Fe_{50}Pt_{50}$ and $Fe_{20}Ni_{80}$ respectively. The comparable values of spin mixing conductance at both interfaces shows a similar rate of spin momentum transfer.

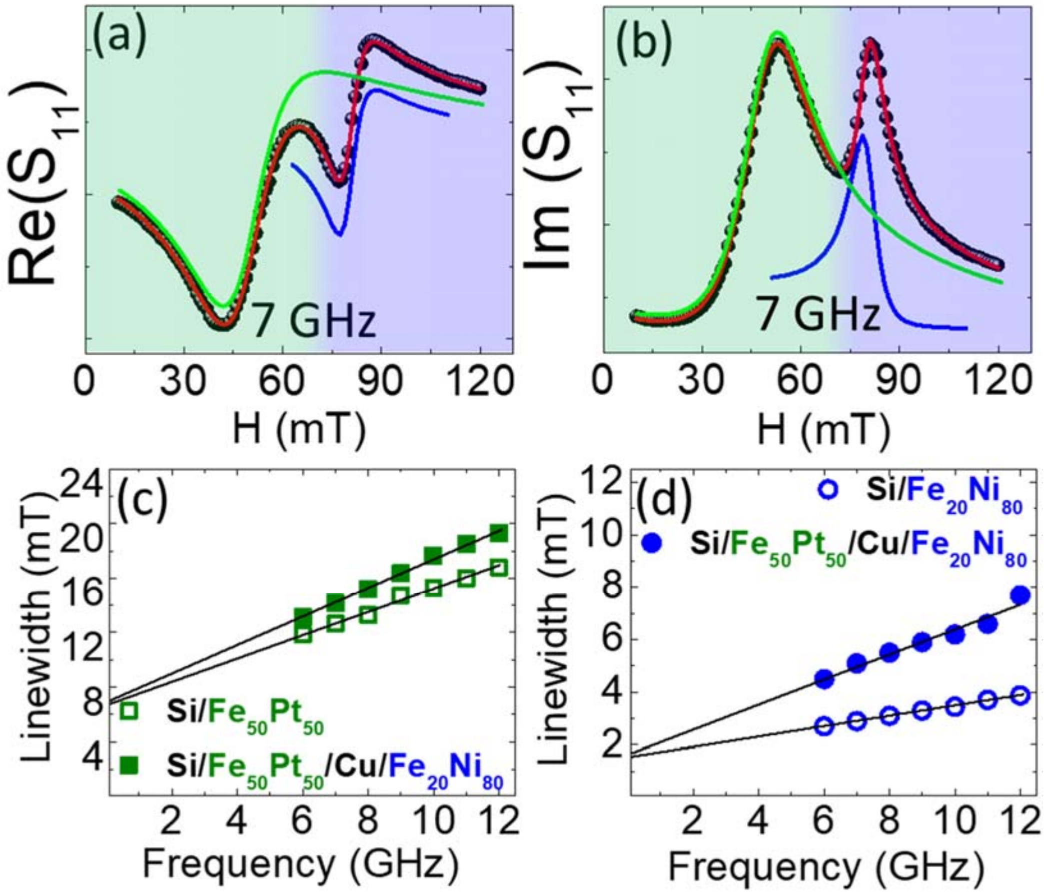

Figure 2. a) Real and b) Imaginary FMR spectrum for $Fe_{50}Pt_{50}/Cu/Fe_{20}Ni_{80}$ for f = 7 GHz for ϕ = 0^{o}. Black solid dots and the Red curve show experimental data and fitted curve using equation 1. Green and Blue curves represent the deconvoluted spectra of respective FM films. Resonance-linewidth as a function of frequency for c) $Fe_{50}Pt_{50}$ and d) $Fe_{20}Ni_{80}$, respectively in trilayer and single layer samples.

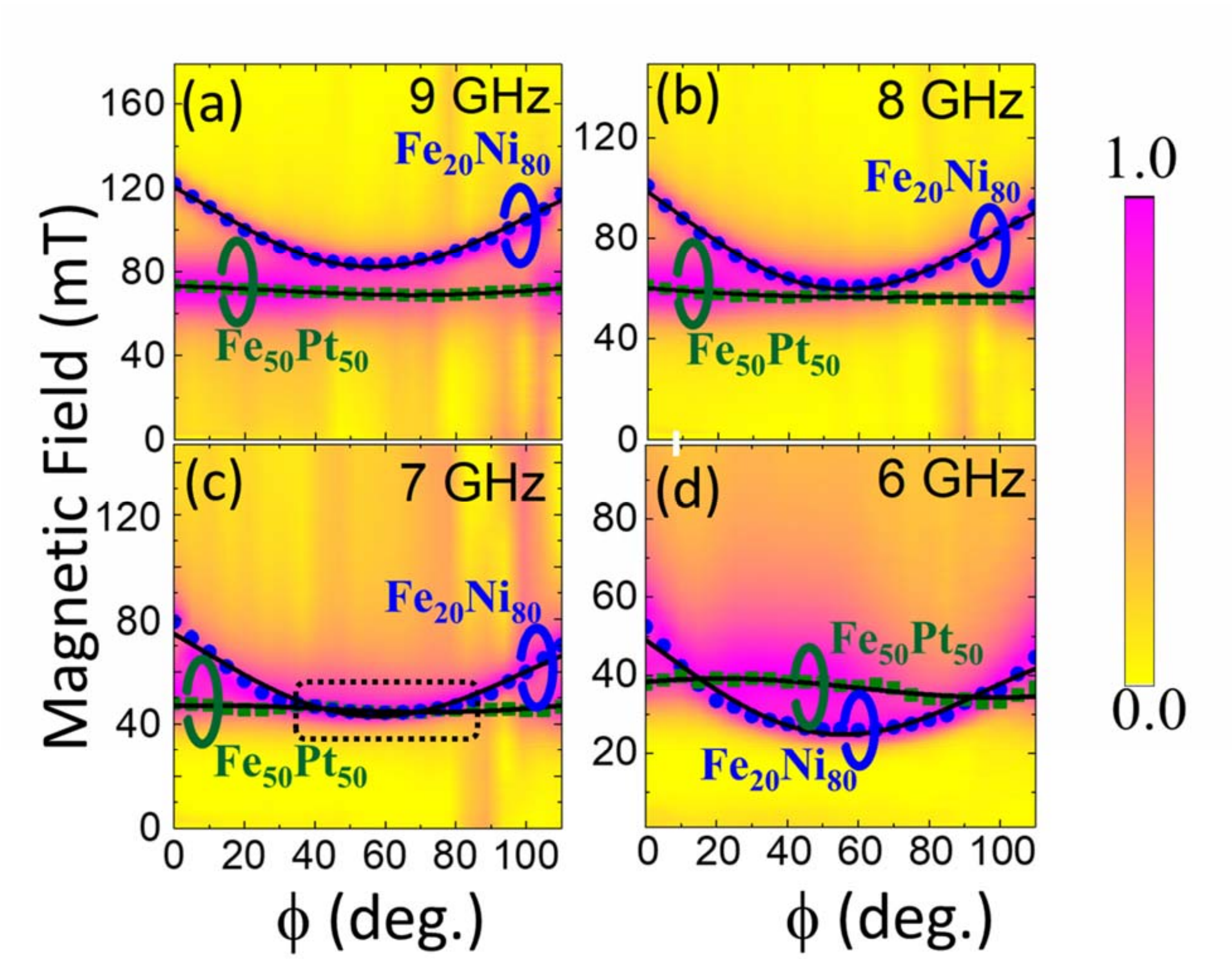

Figure 3. The pseudo-color plot of normalized FMR spectra intensity as a function of the magnetic field and azimuthal angle ϕ for $Fe_{20}Ni_{80}$/Cu/$Fe_{50}Pt_{50}$ trilayer structure recorded at (a) 9 GHz (b) 8 GHz (c) 7 GHz and (d) 6 GHz excitation frequency. Blue solid circles and Green solid squares show the H_R values of $Fe_{20}Ni_{80}$ and $Fe_{50}Pt_{50}$ extracted by equation 1. Solid red lines show the fitting using equation 2.

Next, in-plane FMR spectra are recorded for different azimuthal angle $0 < \phi < 120^o$ at regular interval of 5°. Figure 3 highlights the color representation of the normalized amplitude of the S_{11} signal for all recorded FMR spectra. The two separated magenta-colored curves in Figure

3a indicate that precession at f = 9 GHz occurred in both layers discretely for all the studied ϕ range where large variation in H_R of $Fe_{20}Ni_{80}$ is due to induced in-plane anisotropy. A similar trend is observed for f = 8 GHz, though resonant field for both $Fe_{20}Ni_{80}$ and $Fe_{50}Pt_{50}$ is found to be getting closer for ϕ approx. equal to 55°, evident in Figure 3b. When applied microwave frequency reduced to 7 GHz, H_R is found to be coinciding in the wide region of 25° < ϕ < 80°, implying simultaneous precession of $Fe_{50}Pt_{50}$ and $Fe_{20}Ni_{80}$ depicted in Figure 3c. Thereafter, for f = 6 GHz, both FM layers precess together for certain ϕ configuration only, as observed by two intersections in H_R values, shown in Figure 3d, followed by no such observation of mutual precession for lower frequencies. To provide a better picture of FMR-configuration dependent H_R behavior for $Fe_{50}Pt_{50}$/Cu/$Fe_{20}Ni_{80}$ sample, real and imaginary S_{11} signal at f = 7 GHz for only selected ϕ = 20°, 40°, 60°, 80°, 100° and 120° is also shown in supplementary information [Figure S2]. When angle ϕ lies between 40° to 80°, H_R of both FMR peaks approach to each other signifying that FM layers start resonating collectively at the same external field as visualized by scheme 3 in Figure 1c. Note that chosen ferromagnets i.e. $Fe_{50}Pt_{50}$ and $Fe_{20}Ni_{80}$ exhibits 4 times of difference in linewidth [Figure 2c and 2d] which enables us to estimate both H_R as well as the ΔH unambiguously, even in certain cases of overlapped FMR spectra. While further increase in ϕ beyond 100° leads to dissimilar H_R i.e. $Fe_{50}Pt_{50}$ and $Fe_{20}Ni_{80}$ are now precessing rather independently.

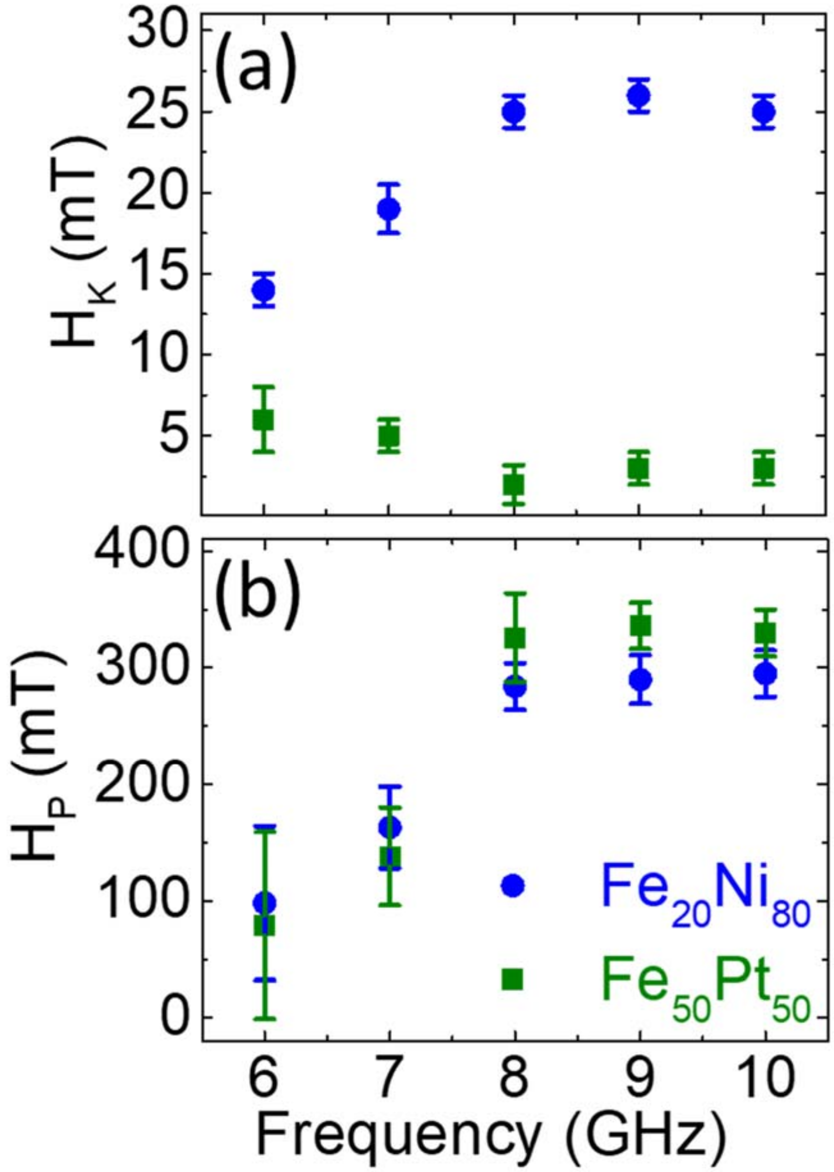

Figure 4. Estimated variation of a) in-plane b) out-of-plane anisotropy field for $Fe_{20}Ni_{80}$ and $Fe_{50}Pt_{50}$ in trilayer plotted for different excitation frequency highlight the modulation in the effective magnetic field due to varying FMR-configurations.

The precessing ferromagnets attached to the NM layer is expected to have spin accumulation at FM/NM interface, may result in the induced effective field [33]. The precessing ferromagnet

$Fe_{50}Pt_{50}$ ($Fe_{20}Ni_{80}$) at their resonance field, will results in the spin accumulation at interface Cu/$Fe_{20}Ni_{80}$ (Cu/$Fe_{50}Pt_{50}$), respectively. When both, ferromagnets are precessing simultaneously at the same resonant field, spin current crossing the Cu/$Fe_{20}Ni_{80}$ and Cu/$Fe_{50}Pt_{50}$ interface cancels, resulting in no spin accumulation. In, a recent report, Hou et al. [34] also showed that spin pumping could generate an effective magnetic field to break time-reversal symmetry at studied YIG/Au interface. Consequently, the angular variation in the effective field ($4\pi M_{eff} = 4\pi M_S - H_P$) for $Fe_{50}Pt_{50}$/Cu/$Fe_{20}Ni_{80}$ sample owing to varying spin-pumping conditions is quantitatively examined. Where ϕ dependence of H_R is fitted using equation 2 as displayed with a black fitting curve in Figure 3 to estimate the modulation in anisotropy fields [35].

$$H_R = -H_K + \frac{3}{2}H_K\sin^2(\phi+\beta) - \frac{1}{2}(4\pi M_S - H_P) + \frac{1}{2}\left[{H_K}^2\sin^4(\phi+\beta) + 4(4\pi M_S - H_P)H_K\sin^2(\phi+\beta) + (4\pi M_S - H_P)^2 + 4\frac{f^2}{\gamma^2}\right]^{\frac{1}{2}} \quad (2)$$

The resulting values of H_P (out-of-plane anisotropy field) and H_K (in-plane anisotropy field) as a function of excitation frequency f for $Fe_{20}Ni_{80}$ and $Fe_{50}Pt_{50}$ are summarized in Figure 4a and 4b respectively, keeping the $4\pi M_S$ values for $Fe_{20}Ni_{80}$ and $Fe_{50}Pt_{50}$ to be reasonably constant as 1000 mT and 1400 mT respectively [refer to supplementary figure S3]. β account for offset in the minima or maxima value in the experimentally obtained angular dependence of resonance field. It shows that H_K and H_P depend largely on spin-pumping conditions like $Fe_{20}Ni_{80}$ featured a drop in H_K for $f < 8$ GHz due to the coupling of magnetization precession while $Fe_{50}Pt_{50}$ show a minor gain of 5 mT. On the contrary, a large decrease in anisotropy H_P, from 290 to 98 mT for $Fe_{20}Ni_{80}$ and from 340 to 68 mT for $Fe_{50}Pt_{50}$ is induced i.e. when they start behaving identically in mutual precession conditions by the exchange of spin-current via Cu insertion layer. Hence, M_{eff} will also be changed by the contribution of H_K and H_P as FMR configuration alters as shown in supplementary figure S4. Interestingly, in Ref. 30, the presence of different material interfaces is also shown to vary the reduction of M_{eff} values with respect to the saturation magnetization M_S of FeNi and CoFeB system.

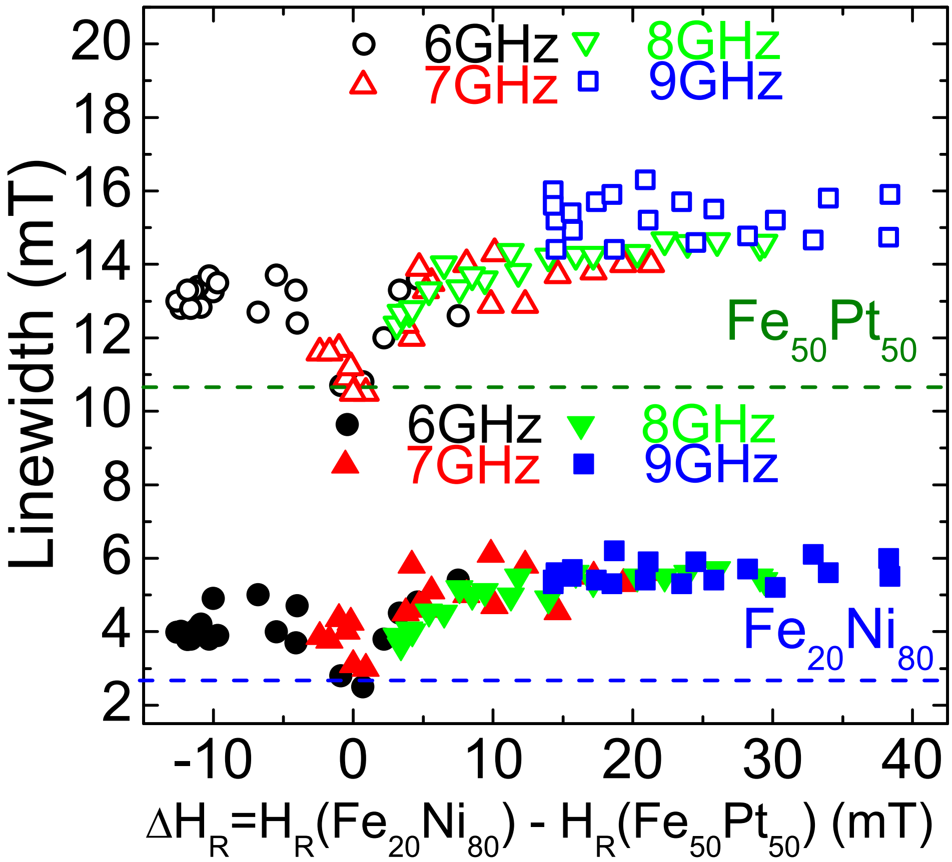

Figure 5. FMR linewidth of FM layers in tri-layer structure plotted as a function of ΔH_R. The dotted lines represent the linewidth obtained for Si/$Fe_{20}Ni_{80}$ and Si/$Fe_{50}Pt_{50}$ samples at 7 GHz.

To elucidate the influence of collective precession on relaxation as well for present tri-layer $Fe_{50}Pt_{50}$/Cu/$Fe_{20}Ni_{80}$ system, FMR absorption linewidth of both $Fe_{20}Ni_{80}$ and $Fe_{50}Pt_{50}$ as a function of ΔH_R (= H_R ($Fe_{20}Ni_{80}$) - H_R ($Fe_{50}Pt_{50}$)) is plotted for frequency 6 to 9 GHz as shown in Figure 5.

The FMR linewidth of Si/$Fe_{20}Ni_{80}$ and Si/$Fe_{50}Pt_{50}$ samples for f = 7GHz are also plotted in Figure 5. In trilayer, for $\Delta H_R \neq 0$ state (i.e. H_R ($Fe_{20}Ni_{80}$) $\neq$ H_R ($Fe_{50}Pt_{50}$)), the effective linewidth of both exclusively resonating ferromagnets showed enhanced values due to spin relaxation. However, at $\Delta H_R \rightarrow 0$ (i.e. H_R ($Fe_{20}Ni_{80}$) $\cong$ H_R ($Fe_{50}Pt_{50}$)), the FMR linewidth of both $Fe_{20}Ni_{80}$ and $Fe_{50}Pt_{50}$ drops to their minimum values that are comparable to intrinsic linewidth as detected from Si/ $Fe_{20}Ni_{80}$ and Si/$Fe_{50}Pt_{50}$ samples. When both ferromagnets are precessing at the identical resonance field, the opposite flow of spin current across both interface $Fe_{50}Pt_{50}$/Cu and Cu/$Fe_{20}Ni_{80}$ is effectively vanishes and thus results into no excess broadening of FMR linewidth [12]. Note that additional FMR measurements at higher excitation frequencies (≥ 9 GHz) didn't show collective dynamics. As predicted by Heinrich et al. [12] that dynamic exchange coupling not only leads to damping modulation, but also new collective behavior of magnetic order parameters is highlighted here and need further studies for better understating.

IV. CONCLUSIONS

We performed angular VNA-FMR measurement to investigate spin pumping effect on magnetization dynamics of asymmetric $Fe_{50}Pt_{50}$/Cu/$Fe_{20}Ni_{80}$ sample, where oblique deposition induced purposeful uniaxial anisotropy of approx. 24 mT in $Fe_{20}Ni_{80}$ allowed us to analyze mutual precession for certain angular FMR-conditions. We observed that anisotropy field can also be effectively modulated in addition to non-local Gilbert damping, with minimizing the spin-pumping effect or in other words by means of changing excitation configurations of studied $Fe_{50}Pt_{50}$/Cu/$Fe_{20}Ni_{80}$ system. Both $Fe_{20}Ni_{80}$ and $Fe_{50}Pt_{50}$ displayed an identical behavior at mutual precession and a significant reduction in anisotropy field, of around 200 mT accompanied by no excess damping due to the effective cancelation of net flow of spin-current. This experimental finding attempts to decipher the less-explored interface effects towards controlling not only static properties but dynamic magnetic order parameters in the variety of spintronic devices often consist of typical FM/NM/FM multilayer stack.

ACKNOWLEDGEMENT

The authors thank to Dr. Hironori Asada for technical discussion and Angshman Deka for his help in FMR measurements. Financial support from JSPS Grant-in-Aid (KAKENHI No. 18H01862, 18H05953) is also gratefully acknowledged. This work is partially supported by Nippon Sheet Glass Foundation. R. M. would like to acknowledge research grant MOE2017-T2-2-129. R. S. R would like to acknowledge research grant NTU Tier 1, RP 2/16 RSR.

References

1. a) E.B. Myers, D.C. Ralph, J.A. Katine, R.N. Louie, R.A. Buhrman, *Science* **1997,** *285*, 867; b) J.A. Katine, F.J. Albert, R.A. Buhrman, E.B. Myers, D.C. Ralph, *Phys. Rev. Lett.* **2000**, *84*, 3149; c) M.A.M. Gijs, G.E.W. Bauer, *Adv. Phys.* **1997,** *46*, 285.
2. a) J.C. Slonczewski, *J. Magn. Magn. Mater.* **1999,** *195*, L261; b) J.C. Slonczewski, *J. Magn. Magn. Mater.* **1996**, *159*, L2.
3. L. Liu, Chi-Feng Pai, Y. Li, H. W. Tseng, D. C. Ralph, R. A. Buhrman, *Science* **2012,** *336*, 6081.
4. G. Yu, P. Upadhyaya, Y. Fan, J. G. Alzate, W. Jiang, K. L. Wong, S. Takei, S. A. Bender, Li-Te Chang, Y. Jiang, M. Lang, J. Tang, Y. Wang, Y. Tserkovnyak, P. K.Amiri, K. L. Wang, *Nat. Nanotechnol.* **2014**, *9*, 548.
5. K. Ando, S. Takahashi, J. Ieda, H. Kurebayashi, T. Trypiniotis, C. H. W. Barnes, S. Maekawa, E. Saitoh, *Nat. Mater.* **2011,** *10*, 655.
6. H. Wang, C. Du, P. C. Hammel, F. Yang, *Phys. Rev. Lett.* **2014**, *113*, 097202.
7. S. Gupta, R. Medwal, D. Kodama, K. Kondou, Y. Otani, Y. Fukuma, *Appl. Phys. Lett.* **2017,** *110*, 022404.
8. T. Kimura, Y. Otani, *Phys. Rev. Lett.* **2007**, *99*, 196604.
9. S. O. Valenzuela, M. Tinkham, *Nature*, **2006**, *442*, 176.
10. C. H. Tsang, R. E. Fontana, T. Lin, D. E. Heim, B. A. Gurney, M. L. Williams, *IBM J. Res. Dev.*, **1998**, *42*, 1.
11. T. J. Silva, W.H. Rippard, *J. Magn Magn. Mater.* **2008**, *320*, 1260.
12. B Heinrich, Y. Tserkovnyak, G. Woltersdorf, A. Brataas, R. Urban, G. E. W. Bauer, *Phys. Rev. Lett.* **2003**, *90*, 187601.
13. R. Salikhov, R. Abrudan, F. Brüssing, St. Buschhorn, M. Ewerlin, D. Mishra, F. Radu, I. A. Garifullin, H. Zabel, *Appl. Phys. Lett.* **2011**, *99*, 092509.
14. R. Salikhov, R. Abrudan, F. Brussing, K. Gross, C. Luo, K. Westerholt, H. Zabel, F. Radu, I. A. Garifullin, *Phys. Rev. B* **2012**, *86*, 144422.
15. Y. Li, W. Cao, W. E. Bailey, *Phys. Rev. B* **2016**, *94*, 174439.
16. A. A. Baker, A. I. Figueroa, C. J. Love, S. A. Cavill, T. Hesjedal, G. van der Laan, *Phys. Rev. Lett.* **2016**, *116*, 047201.
17. H. Yang, Y. Li, W. E. Bailey, *Appl. Phys. Lett.* **2016**, *108*, 242404.
18. a) Y. Tserkovnyak, A. Brataas, G. E. W. Bauer, *Phys. Rev. Lett.* **2002**, *88*, 117601; b) B. Heinrich, G. Woltersdorf, R. Urban, E. Simanek, *J. Appl. Phys.* **2003**, *93*, 7545.
19. Y. Pogoryelov, M. Pereiro, S.Jana, A.Kumar, S. Akansel, M. Ranjbar, D. Thonig, P. Svedlindh, J. Akerman, O. Eriksson, O. Karis, D. A. Arena, arxiv.org/abs/1812.09978
20. Y. Tserkovnyak, Doctoral Thesis, Harvard University **2003**.
21. C. J. Durrant, L. R. Shelford, R. A. J. Valkass, R. J. Hicken, A. I. Figueroa, A. A. Baker, G. van der Laan, L. B. Duffy, P. Shafer, C. Klewe, E. Arenholz, S. A. Cavill, J. R. Childress, J. A. Katine, *Phys. Rev. B* **2017**, *96*, 144421.
22. R. Gupta, N. Sehdev, K. Asokan, D. Kanjilal, S. Annapoorni, *J. Appl. Phys.* **2014**, *116*, 083902.
23. Y. Fukuma, Z. Lu, H. Fujiwara, G. J. Mankey, W. H. Butler, S. Matsunuma, *J. Appl. Phys.* **2009,** *106*, 076101.
24. R. D. McMichael, C. G. Lee, J. E. Bonevich, P. J. Chen, W. Miller, W. F. Egelhoff, *J. Appl. Phys.* **2000**, *88*, 5296.

25. J. Bass, W. P. P. Jr, *J. Phys.: Condens. Matter*. **2007**, *19*, 183201.
26. S. S. P. Parkin, R. Bhadra, K. P. Roche, *Phys. Rev. Lett.* **1991**, *66*, 2152.
27. P. Bruno, *Euro. Phys. Lett.* **1993**, *23*, 615.
28. S. Gupta, D. Kumar, T. L. Jin, R. Nongjai, K. Asokan, A. Ghosh, M. Aparnadevi, P. Suri, S. N. Piramanayagam, *AIP Adv.* **2018**, *8*, 056125.
29. B. Heinrich, J. F. Cochran, R. Hasegawa *J. Appl. Phys.* **1985**, *57*, 3690.
30. A. R. Calaforra, T. Bracher, V. Lauer, P. Pirro, B. Heinz, M. Geilen, A. V. Chumak, A. Conca, B. Leven, B. Hillebrands, *J. Appl. Phys.* **2015**, *117*, 163901.
31. N. Alvarez, G. Alejandro, J. Gomez, E. Goovaerts, A. Butera, J. *Phys. D: Appl. Phys.* **2013**, *46*, 505001.
32. T. Seki, Y. Hasegawa, S. Mitani, S.Takahashi, H. Imamura, S. Maekawa, J. Nitta, K.Takanashi, *Nat. Mater.* **2008**, *7*, 125.
33. A. Manchon, J. Zelezný, I.M. Miron, T. Jungwirth, J. Sinova, A. Thiaville, K. Garello, P. Gambardella, arXiv:1801.09636v2
34. D. Hou, Z. Qiu, R. Iguchi, K. Sato, E. K. Vehstedt, K. Uchida, R.E.W. Bauer, E. Saitoh, *Nat. Comm.* **2016**, *7*, 12265.
35. R. A. Gallardo, S. Khanal, J. M. Vargas, L. Spinu, C. A. Ross, C. Garcia, *J. Phys. D: Appl. Phys.* **2017**, *50*, 075002.